



## Efficient Computational Method for Ballistic Currents and Application to Single Quantum Dots

M. SABATHIL AND S. BIRNER

*Walter Schottky Institute, Technische Universität München, Am Coulombwall 3, 85748 Garching, Germany*

D. MAMALUY

*Department of Electrical Engineering, Arizona State University, Tempe, AZ 85287-5706, USA*

P. VOGL

*Walter Schottky Institute, Technische Universität München, Am Coulombwall 3, 85748 Garching, Germany*

**Abstract.** We present an efficient method for the calculation of the ballistic transmission function and current through an arbitrarily shaped, multi-terminal two- or three-dimensional open device. The method is applicable to cases where a ballistic current model is meaningful and charge self-consistency is not relevant, such as quantum dot devices, quantum wires, or interferometer type of structures. As a concrete example, we study the electron escape rate in self-assembled GaAs/InGaAs single quantum dots as a function of applied bias, as measured by photocurrent experiments.

**Keywords:** ballistic transport, quantum dots, nanometer device simulation

### 1. Introduction

In recent years, zero dimensional heterostructures such as quantum dots (QD) became a subject of increasing attention experimentally as well as theoretically. So far, most theoretical studies have focused on the static electronic and optical properties of these atom-like structures. On the other hand, many experimental groups investigate the transport properties of open quantum dot devices either by resonant tunneling experiments [1–5] or in photocurrent experiments [6–8]. The calculation of the tunneling transport of electrons and holes through a realistic QD coupled to external leads is extremely difficult and is basically out of reach with present-day methods. Thus, the transport calculations that have been published so far either considered simplified geometries [9–11] or very small structures [12].

Recently, we have developed an efficient method to calculate the ballistic transmission function and current

through an arbitrarily shaped, multi-terminal two- or three-dimensional open device [13]. This method, that we have termed contact block reduction (CBR) method, allows us to study the transport properties of realistic quantum dot structures. It is applicable to all cases where the current is sufficiently small so that a ballistic model is meaningful and charge self-consistency is not relevant. This is the case for many quantum dot devices, quantum wires, or interferometer type of structures.

With the widely used QTBM [14,15] method, the computational effort for the calculation of the ballistic current through a 3D device of complex geometry scales with the third power of the number of nodes or grid points covering the entire device. This requires the repeated inversion of matrices of typical size  $10^5$ – $10^6$  for each energy step. In the CBR method, on the other hand, this effort can be reduced to a single calculation of a small percentage of the stationary states in the isolated device plus the inversion of a small matrix that is

governed by the number of propagating modes in the leads.

In this paper, we first exemplify the CBR method by studying tunneling through buried model quantum dots mainly to illustrate the convergence of the method. Secondly, we predict the escape rates of captured electrons in realistic overgrown self-assembled GaAs/InGaAs quantum dot structures for various shapes and alloy profiles and compare to recent experimental results [6].

## 2. Contact Block Reduction Method

In this section we briefly review the CBR method [13] and use the device depicted in Fig. 1 to illustrate the main ingredients. We assume Dirichlet boundary conditions at the side walls, such that the current is one-dimensional in the  $z$ -direction. The scattering region in the middle section contains the barrier potential and a cuboidally shaped quantum dot. The two leads are assumed to continue infinitely to the right and left, respectively. Within the leads, the Schrödinger equation is assumed to be separable so that the propagating solutions have the form  $\psi_m(r_{\parallel}, z; E) = e^{ik_z(E,m)z} \chi_m(r_{\parallel})$  with  $k_z$  real and the transverse modes  $\chi_m(r_{\parallel})$  resulting from the two-dimensional lateral Schrödinger equation across the leads. According to the Landauer-Büttiker formalism, the current from lead  $\lambda$  to lead  $\lambda'$  can be expressed in terms of the transmission function  $T_{\lambda\lambda'}(E)$  and the distribution functions of the leads. The transmission function can be obtained from the retarded Green's function  $G^R$  of the open device (see, e. g. [16]):

$$T_{\lambda\lambda'} = \text{Tr}(\Gamma_{\lambda} G^R \Gamma_{\lambda'} G^A),$$

$$\Gamma_{\lambda} = i(\Sigma_{\lambda} - \Sigma_{\lambda}^{\dagger}).$$

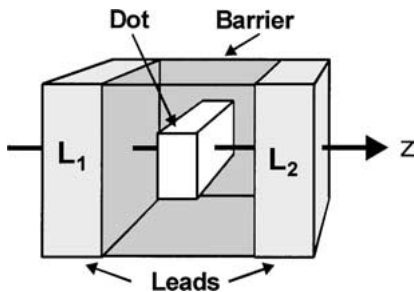


Figure 1. Model dot structure with outer dimensions of  $40 \times 40 \times 20$  nm with 2 semi-infinite leads and the interior containing a tunneling barrier region and a cuboidally shaped quantum dot.

The coupling to the leads is introduced via the self-energy matrix  $\Sigma$ . We now consider separately the problem of a closed system (decoupled device) that is described by a Hermitian Hamiltonian  $H^0$ , and the coupling  $\Sigma$  to the attached leads. The retarded Green's function  $G^R$  can be calculated via the Dyson equation

$$G^R = [\mathbf{I} - G^0 \Sigma]^{-1} G^0. \quad (1)$$

The key point of the CBR method is that the size of the determinant  $\det(\mathbf{I} - G^0 \Sigma)$  is governed by the size of  $\Sigma$  that is small and nonzero only at the contacts. Thus, the Green's function of the decoupled device,

$$G^0(E) = [E\mathbf{I} - H^0]^{-1} = \sum_{\alpha} \frac{|\psi_{\alpha}\rangle\langle\psi_{\alpha}|}{E - E_{\alpha}}, \quad (2)$$

is only needed at the contacts. The eigenfunctions are obtained by solving the Schrödinger equation of the decoupled device once for all, employing von Neumann boundary conditions at the contacts. The use of these boundary conditions grossly reduces the needed range of the eigenvalue spectrum of  $H^0$  in the calculation of the transmission function; a few percent of the eigenvalues are usually sufficient. The remaining task of solving the Dyson equation for each energy is also reduced (typically by an order of magnitude) by the fact that only propagating modes need to be taken into account in  $T(E)$ .

In passing we note that the CBR method is similar to the R-matrix method [9,17] that is known from atomic physics, but the present method can be applied to any type of self-energy matrix and allows a straightforward generalization of the formalism to the multi-band case.

## 3. 3D Model Dot Resonant Tunneling Structure

We first calculated the transmission through a model quantum dot resonant tunneling structure depicted in Fig. 1. There is a cuboidal dot of 14 nm lateral diameter and 5 nm thickness embedded within a 15 nm thick barrier region. For the calculation we used a one-band Hamiltonian with an electron mass of  $0.067 [m_0]$  and barrier heights of 0.4 eV. The potential has been set to zero in the leads and to  $-0.2$  eV within the dot. The total size of the device region is  $40 \times 40 \times 20$  nm. With a grid spacing of 1 nm, this leads to a matrix size of 35000 for  $H^0$ . To check the convergence with respect to the number of eigenstates included in Eq. (2), we have calculated the transmission function for zero

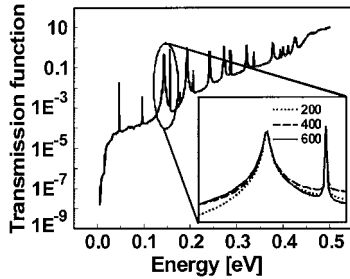


Figure 2. Transmission function versus energy in eV for the structure depicted in Fig. 1. The inset shows the result when 200, 400, or 600 eigenstates are included in the calculation of the Green's function of the decoupled device in Eq. (2), respectively.

applied bias including 200, 400 and 600 eigenstates, respectively (Fig. 2).

The inset in Fig. 2 shows that the peak values of the transmission are well converged already with very few eigenstates, whereas the non-resonant part of  $T(E)$  converges rather slowly. Indeed, only a single resonant eigenstate contributes to the transmission close to the corresponding pole of  $\mathbf{G}^0$  whereas all eigenstates contribute otherwise, with a weight that is inversely proportional to the energy. Fortunately, the current is dominated by the peak values of  $T(E)$  so that the  $I$ - $V$  characteristics is insensitive to the number of eigenvalues included. The limiting factor in our calculations is the storage rather than the computer time for the diagonalization of the sparse matrix  $\mathbf{H}^0$ . In Fig. 3, we show the calculated ballistic current, where we assumed a Fermi level of 60 meV and zero temperature in each lead.

We note that the chosen total lateral size of the device in Fig. 1 (40 nm) is sufficiently large so that it does not influence the transmission and the current through the dot. We checked this explicitly by repeating the calculation for a 60 nm wide device.

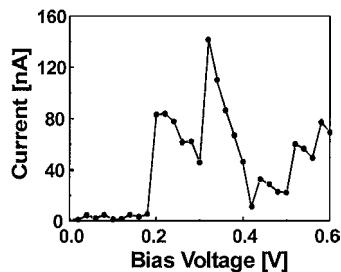


Figure 3. The ballistic current through the model quantum dot structure shown in Fig. 1, assuming a Fermi level of 60 meV in each lead and zero temperature.

#### 4. Electron Escape Rate in InGaAs-Quantum Dots

Several experimental groups [6–8] have fabricated Schottky diode structures with embedded self-assembled InGaAs quantum dots and have been able to perform photocurrent measurements on single dots as a function of the applied voltage. If this voltage is sufficiently large, the resonantly generated exciton gets ionized and the electron tunnels out of the dot before the exciton can recombine radiatively. Therefore, the line width of the exciton absorption is a measure of its decay rate via recombination and tunneling escape [6–8]. We will specifically focus on the device structure fabricated by Oulton *et al.* [6] that show a zero-field exciton energy of 1.255 eV.

We have implemented the CBR method into our nanodevice simulation tool *nextnano*<sup>3</sup> [18–20]. This enables us to investigate the tunneling rate through realistic quantum dot structures for various dot shapes and alloy profiles including the GaAs substrate and a 1 nm thick  $\text{In}_{0.4}\text{Ga}_{0.6}\text{As}$  wetting layer. The strain is calculated via minimization of the elastic energy; the resulting band shifts and splittings and the piezoelectric charges are fully taken into account. By applying appropriate boundary conditions to the total structure, the width of the resonance peak is equivalent to the decay rate of the quasi bound states inside the quantum dot.

Concretely, Fig. 4 shows a cross section of the band edge states near the InGaAs quantum dot region and cutting through the center of the dot, for an electric field of 100 kV/cm. The wetting layer is 1 nm thick and consists of  $\text{In}_{0.4}\text{Ga}_{0.6}\text{As}$ . TEM measurements suggest an approximate dot height of 4 nm.

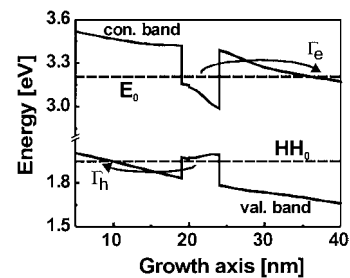


Figure 4. Conduction and valence band edge for a slice through the center of a 4 nm high InGaAs quantum dot with linear alloy profile grown on a 1 nm thick wetting layer. The applied field is 100 kV/cm. The electron state in the quantum dot can escape with a rate  $\Gamma_e$  to the right as indicated schematically in the figure. Analogously, the hole may escape to the left with a rate  $\Gamma_h$ .

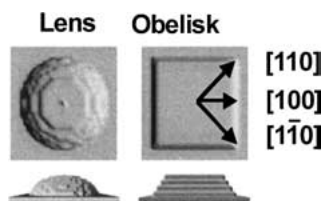


Figure 5. The two principally different types of dot shapes that are considered in the present calculations. The lateral diameter of the lens-shaped dot and the obelisk is taken as 22 and 20 nm, respectively.

Keeping the zero field exciton energy equal to the measured one, we have investigated the tunneling through dots of two principally different shapes, a lens and a truncated pyramid (obelisk) namely (see Fig. 5) and we have taken heights of 3 nm and 4 nm in both cases. In one case, we have assumed a trumpet-shaped alloy profile [21]; since its effect on the electron tunneling rate is small, we have used a linear alloy profile with increasing Indium content towards the tip of the dot in all other cases.

The computational effort amounts to the following. First, we find approximately the 300 to 400 lowest eigenstates of the Hamiltonian of total dimension  $N \sim 80000$ . In the small energy interval close to the ground state of the quantum dot that is relevant for the tunneling out of the dot, only very few lead-modes propagate. Therefore, the dimension of the matrix that has to be inverted for each energy is smaller than 100. As a consequence, the computational costs are dominated by the solution of the eigenvalue problem.

In Fig. 6, we compare our theoretical results with the experimental data. Shown are the predicted line widths of the various dots that we have investigated, compared to the experimental values. All theoretical

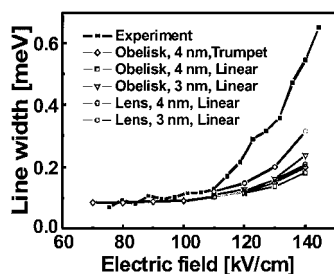


Figure 6. The experimentally measured exciton line width is plotted as a function of the applied electric field (full squares, Ref. [6]) and compared with the present theoretical calculations for various quantum dot shapes (obelisk or lens), heights (4 nm or 3 nm), and alloy profiles (trumpet or linear).

data have been shifted by an offset of 0.085 meV that is equal to the observed zero-field line width [6]. Since the tunneling rates depend exponentially on the barrier heights which in turn depend on band offsets that are not accurately known, the agreement between theory and experiment is only semi-quantitative. Nevertheless, the comparison clearly shows that lens-shaped and thinner quantum dots exhibit significantly higher tunneling rates than pyramidal and thicker dots.

## 5. Conclusion

We have shown that the CBR method can be successfully and efficiently applied to study realistic three-dimensional quantum devices. It enables one to calculate the ballistic transport properties of much larger systems than previously and allows for the detailed investigation of properties such as tunneling rates and current-voltage characteristics.

## Acknowledgments

This work was supported by ONR contract N00014-01-1-0242 and the Deutsche Forschungsgemeinschaft.

## References

1. K.H. Schmidt, M. Versen, C. Bock, U. Kunze, D. Reuter, and A.D. Wieck, *Physica E*, **7**, 425 (2000).
2. M. Narihito, G. Yusa, Y. Nakamura, T. Noda, and H. Sakaki, *Appl. Phys. Lett.*, **70**, 105 (1997).
3. T. Bryllert, M. Borgstrom, T. Sass, B. Gustafson, L. Landin, L.-E. Wernersson, W. Seifert, and L. Samuelson, *Appl. Phys. Lett.*, **80**, 2681 (2001).
4. M. Versen, K.H. Schmidt, C. Bock, D. Reuter, A.D. Wieck, and U. Kunze, *Phys. Stat. Sol.*, (b) **224**, 669 (2001).
5. I.E. Itskevich, T. Ihn, A. Thornton, M. Henini, T.J. Foster, P. Moriarty, A. Nogaret, P.H. Beton, L. Eaves, and P.C. Main, *Phys. Rev. B* **54**, 16401 (1996).
6. R. Oulton, J.J. Finley, A.D. Ashmore *et al.*, *Phys. Rev. B*, **66**, 045313 (2002).
7. E. Beham, A. Zrenner, F. Findeis, M. Bichler, and G. Abstreiter, *Appl. Phys. Lett.*, **79**, 2808 (2001).
8. P.W. Fry, J.J. Finley, L.R. Wilson *et al.*, *Appl. Phys. Lett.*, **77**, 4344 (2000).
9. E. Onac, J. Kucera, and U. Wulf, *Phys. Rev. B* **63**, 085319 (2001).
10. Shu-Shen Li, Ahmad Abliz, Fu-Hua Yang, Zhi-Chuan Niu, Song-Lin Feng, Jian-Bai Xia, and Kenji Hirose, *J. Appl. Phys.*, **92**, 6662 (2002).
11. D.M.-T. Kuo and Yia-Chung Chang, *Phys. Rev. B*, **61**, 11051 (2000).
12. Y.M. Niquet, C. Delerue, M. Lannoo, and G. Allan, *Phys. Rev. B*, **64**, 113305 (2001).

13. D. Mamaluy, M. Sabathil, and P. Vogl, *J. Appl. Phys.*, **93**, 4628 (2003).
14. Craig S. Lent and David J. Kirkner, *J. Appl. Phys.* **67**, 6353 (1990).
15. D.Z.-Y. Ting, E.T. Yu, and T.C. McGill, *Phys. Rev. B*, **45**, 3583 (1992).
16. S. Datta, *Electronic Transport in Mesoscopic Systems* (Cambridge University Press, Cambridge, UK, 1995).
17. U. Wulf, J. Kucera, P.N. Racec, and E. Sigmund, *Phys. Rev. B*, **58**, 16209 (1998).
18. M. Sabathil, S. Hackenbuchner, J.A. Majewski, G. Zandler, and P. Vogl, *J. Comput. Electronics*, **1**, 81 (2002).
19. S. Hackenbuchner, M. Sabathil, J.A. Majewski, G. Zandler, P. Vogl, E. Beham, A. Zrenner, and P. Lugli, *Physica B*, **314**, 145–149 (2002).
20. The program is freely available, see <http://www.wsi.tu-muenchen.de/nextnano3/>
21. M.A. Migliorato, A.G. Cullis, M. Fearn, and J.A. Jefferson, *Phys. Rev. B*, **65**, 115316 (2002).